Research Article | Open Access

Soft Science

Wu et al. Soft Sci. 2026, 6, 81 DOI:10.20517/ss.2026.96

Vapor-deposited cerium-based halide-organic composites for flexible white electroluminescence

Xingyou Wu[1,#], Jinghui Li[2,#], Zheyu Li[1], Longbo Yang[1], Yiqi Luo[1], Jiajun Luo[1,*], Juan Du[2,*], Jiang Tang[1,3,*]

Keywords: Rare-earth electroluminescence, white light-emitting diodes, flexible display

Citation: Wu, X.; Li, J.; Li, Z.; Yang, L.; Luo, Y.; Luo, J.; Du, J.; Tang, J. Vapor-deposited cerium-based halide-organic composites for flexible white electroluminescence. *Soft Sci.* **2026**, *6*, 81. https://dx.doi.org/10.20517/ss.2026.96

Received: 30 Apr 2026 **First Decision:** 12 Jun 2026 **Revised:** 12 Jul 2026 **Accepted:** 5 Aug 2026 **Published:** 7 Sep 2026

Academic Editor: Chuanfei Guo **Copy Editor:** Pei-Yun Wang **Production Editor:** Pei-Yun Wang

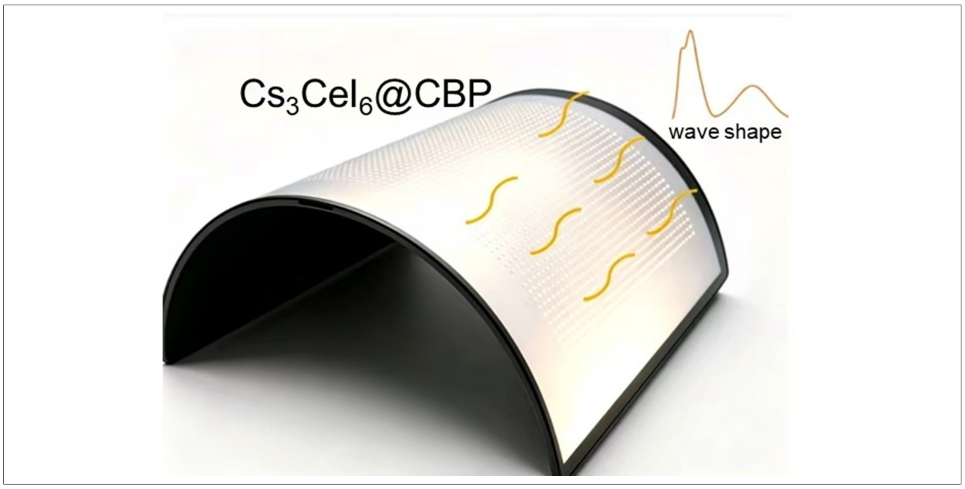

Abstract

White light-emitting diodes (WLEDs) with a single emissive material hold great promise for next-generation lighting, display, and flexible optoelectronic applications. However, it remains difficult to achieve broadband white electroluminescence and efficient carrier utilization within a single emissive material. Here, we report vapor-deposited cerium-based halide-organic composites prepared by multi-source thermal co-evaporation for warm-white electroluminescence. The resulting films exhibit dual-band emission, with a blue band centered at 405 nm and a yellow band centered at 560 nm. Spectroscopic analysis suggests that the blue emission arises from the combined contributions of the Cs_3CeI_6 component and 4,4′-Bis(N-carbazolyl)-1,1′-biphenyl (CBP) fluorescence, whereas the yellow emission is associated with Ce^{3+}-centered 5d–4f emission under a modified local environment induced by interfacial interaction with CBP. Based on these films, warm-WLEDs were fabricated using Cs_3CeI_6@CBP as the emissive layer. The optimized device shows Commission Internationale de l'Eclairage coordinates of (0.38, 0.39), a peak

[1]Wuhan National Laboratory for Optoelectronics (WNLO) and School of Optical and Electronic Information, Huazhong University of Science and Technology (HUST), Wuhan 430074, Hubei, China.
[2]School of Physics and Optoelectronic Engineering, Hangzhou Institute for Advanced Study, University of Chinese Academy of Sciences, Hangzhou 310024, Zhejiang, China.
[3]Optics Valley Laboratory, Wuhan 430074, Hubei, China.
[#]These authors contributed equally to this work.

[*]**Correspondence to:** Prof. Jiajun Luo, Prof. Jiang Tang, Wuhan National Laboratory for Optoelectronics (WNLO) and School of Optical and Electronic Information, Huazhong University of Science and Technology (HUST), Wuhan 430074, Hubei, China. E-mail: luojiajun@mail.hust.edu.cn; jtang@mail.hust.edu.cn; Prof. Juan Du, School of Physics and Optoelectronic Engineering, Hangzhou Institute for Advanced Study, University of Chinese Academy of Sciences, Hangzhou 310024, Zhejiang, China. E-mail: du@ucas.ac.cn

external quantum efficiency of 2.1%, a maximum luminance of 2,678 cd/m^2, and stable electroluminescence spectra over a broad operating-voltage range. Furthermore, proof-of-concept flexible devices fabricated on polyethylene naphthalate substrates retain stable emission under bending conditions, highlighting the potential of these co-evaporated composite films for flexible light-emitting applications. This work establishes a facile and viable strategy to construct cerium-based halide–organic composite films via thermal co-evaporation for efficient warm-white electroluminescence and flexible light-emitting devices.

INTRODUCTION

White light-emitting diodes (WLEDs) are important solid-state light sources for lighting, display, and emerging flexible optoelectronic technologies because they can provide high efficiency, tunable spectra, and good color quality[1-4]. Among different material and device strategies, emissive films that generate broadband white electroluminescence within a single deposited layer are particularly attractive because they can simplify device structures, reduce interfacial complexity, and improve spectral stability[5-8]. Despite substantial progress in perovskites[9,10], organic emitters[11,12], metal complexes[13], and colloidal quantum dots[14], it remains challenging to combine broad visible emission, efficient electrical excitation, and flexible device performance in one material system.

Lanthanide-based materials (e.g., Ce^{3+} and Eu^{2+}) are attractive candidates for white electroluminescence due to their parity-allowed 5d–4f transitions, broadly tunable emission across the visible spectrum, near-unity exciton utilization efficiency, and nanosecond-scale decay lifetimes[15-17]. However, the direct implementation of lanthanide ions in electrically driven LEDs faces several fundamental limitations. On the one hand, the emission of individual lanthanide centers is often insufficiently broad for balanced white-light generation. On the other hand, direct electrical excitation remains difficult because the inner 4f orbitals are shielded by the outer 5s/5p electrons[18,19], which limits carrier injection and energy utilization efficiency. These issues make it difficult to simultaneously achieve broad spectra and efficient electroluminescence in Lanthanide-based systems[20].

To address these limitations, it is desirable to construct co-deposited inorganic–organic films in which the lanthanide-based component provides the luminescent center, while the organic component helps regulate the local coordination environment and excitation process[21,22]. In this context, vacuum thermal evaporation is particularly suitable because it offers solvent-free processing, precise thickness control, and excellent reproducibility[23]. More importantly, multi-source co-evaporation enables accurate regulation of inorganic and organic components in the same film, which is valuable for building compositionally tunable lanthanide-based halide-organic composites and integrating them into light-emitting devices[24-27]. These features make vapor-deposited emissive films promising for flexible optoelectronic applications.

In this work, we develop vapor-deposited cerium-based halide-organic composites for warm-white electroluminescence. By combining the Cs_3CeI_6 with 4,4′-Bis(N-carbazolyl)-1,1′-biphenyl (CBP) in a co-evaporated film, dual-band visible emission is achieved, including a blue band centered at 405 nm and a yellow band centered at 560 nm. Spectroscopic results suggest that the blue emission arises from the combined contributions of Cs_3CeI_6 and CBP fluorescence, whereas the yellow emission is associated with Ce^{3+}-centered 5d–4f emission under a modified local environment induced by interfacial interaction with CBP. Based on these films, warm-WLEDs with Commission Internationale de l'Eclairage coordinates of (0.38, 0.39), a peak external quantum efficiency of 2.1%, and a maximum luminance of 2,678 cd/m^2 are realized. In addition, the flexible electroluminescent device demonstration highlights the potential of these vapor-deposited cerium-based halide-organic composites for flexible light-emitting applications[28].

EXPERIMENTAL

Materials

Cerium iodide (CeI_3, 99.9%) was purchased from Xiong'an Rare Earth Functional Materials Innovation Center Co., Ltd. Cesium iodide (CsI, 99.999%), molybdenum oxide (MoO_3, 99.9%), and lithium fluoride (LiF, 99.9%) were purchased from Sigma-Aldrich. CBP, 3,3′-Bis(carbazol-9-yl)biphenyl (mCBP), 4,4′,4″-Tris(carbazol-9-yl)triphenylamine (TCTA), 1-Bis[4-[N,N-di(4-tolyl)amino]phenyl]-cyclohexane (TAPC), 1,3,5-Tris(1-phenyl-1H-benzimidazol-2-yl)benzene (TPBi), 2,3,6,7,10,11-Hexacyano-1,4,5,8,9,12-hexaazatriphenylene (HAT-CN) and 1,3,5-Tri(m-pyridin-3-ylphenyl)benzene (Tmpypb) were purchased from Xi'an Polymer Light Technology Co., Ltd. Metallic aluminum (Al, 99.99%) was purchased from ZhongNuo Advanced Material Technology Co., Ltd.

Cs_3CeI_6@CBP film fabrication

The Cs_3CeI_6@CBP film was fabricated through thermal co-evaporation using an ultra-high vacuum system (< 1×10^{-4} Pa) with class 1000 cleanroom compatibility. Three independently controlled evaporation sources (CsI, CeI_3, and CBP) were powered by TDK-Lambda precision deposition controllers. Prior to deposition, individual material deposition rates were calibrated via single-source evaporation to establish thickness scaling coefficients (0.04 ± 0.002 Å/s for CsI and 0.02 ± 0.002 Å/s for CeI_3, 2.0 ± 0.1 Å/s for CBP). Real-time rate monitoring was achieved through independent quartz crystals for monitoring with 0.001 Å/s resolution. Comparative ligand systems (mCBP and TCTA) were purchased from Xi'an Polymer Light Technology Co., Ltd. and used as received.

LEDs fabrication and measurement

Patterned indium tin oxide (ITO) substrates (Advanced Electric Technology Co., China) underwent sequential ultrasonic cleaning with detergent, acetone, deionized water, and anhydrous ethanol, followed by oxygen plasma treatment, prior to *in situ* loading into a glovebox-integrated thermal evaporation system (QHV-R197, Shenyang Qihui Vacuum Technology Co., Ltd.). Using a stainless-steel shadow mask under ultrahigh vacuum (< 1×10^{-4} Pa), we sequentially deposited HAT-CN (3 nm), TAPC:15%MoO_3 (40 nm), CBP (5 nm), Cs_3CeI_6@CBP (30 nm), TPBi (25 nm), LiF (2 nm), and Al (100 nm). All LED device characterizations were carried out in a nitrogen-filled glovebox directly connected to the thermal evaporation system. The LED device emitting area was defined as 0.04 cm^2, determined by the overlapping area of ITO and Al electrodes. The J-V, L-V, and external quantum efficiency (EQE) curves were simultaneously recorded using a commercial measurement system (XPQY-EQE, Guangzhou Xi Pu Optoelectronics Tech. Co., Ltd.), equipped with an integrating sphere and photodetector arrays. The operating lifetime, quantified by the temporal evolution of luminance, was also measured using the same system.

Other characterizations

X-ray diffraction (XRD): Patterns were recorded on a PANalytical B.V. X'Pert Pro diffractometer with Cu Kα radiation (λ = 1.54 Å). Thickness of the prepared films used for testing was 200 nm. X-ray photoelectron spectroscopy (XPS): Analysis was conducted using an AXIS-ULTRA DLD-600W spectrometer. Thickness of the prepared films used for testing was 100 nm. Steady-state and time-resolved photoluminescence (TRPL) spectra, photoluminescence quantum yield (PLQY), and decay curves were measured with an OmniFluo 900 system (Zolix), calibrated using a standard halogen lamp. Thickness of the prepared films used for testing was 50 nm.

Transmission electron microscopy (TEM): Samples were prepared by depositing Cs_3CeI_6@CBP directly onto copper mesh substrates. Imaging and elemental mapping were performed on a JEM-ARM200CF microscope equipped with a double Cs-corrector and segmented STEM detector. Thickness of the prepared films used for testing was 50 nm.

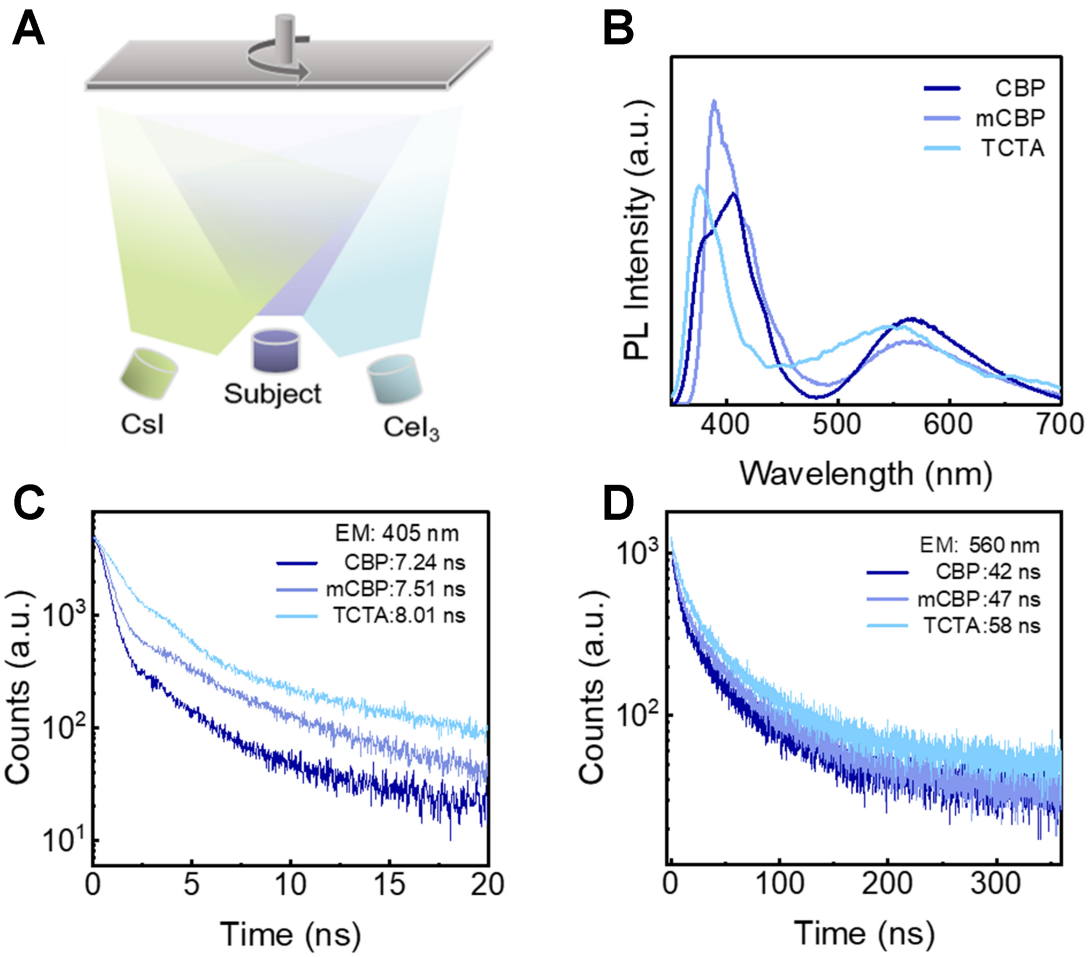

Figure 1. (A) Schematic illustration of the three-source co-evaporation process used to prepare cerium-based halide-organic composites; (B) PL spectra of cerium-based halide-organic composites films under 350 nm excitation; (C) TRPL decay curves of cerium-based halide-organic composites under 350 nm excitation with monitoring at 405 nm; (D) TRPL decay curves of the same films monitored at 560 nm. PL: Photoluminescence; TRPL: time-resolved photoluminescence; CBP: 4,4′-Bis(N-carbazolyl)-1,1′-biphenyl; mCBP: 3,3′-Bis(carbazol-9-yl)biphenyl; TCTA: 4,4′,4″-Tris(carbazol-9-yl)triphenylamine; EM: emission.

RESULTS AND DISCUSSION

To evaluate the luminescent properties of vapor-deposited cerium-based halide-organic composites, we first carried out steady-state photoluminescence (PL), PLQY, and TRPL measurements. A host-screening study was initially performed to identify suitable organic components for co-evaporated Cs_3CeI_6 films. Six conventional organic charge-transport materials were selected, including hole-transport and electron-transport molecules with representative diphenylamine, carbazole, pyrazole, and benzimidazole motifs. These host candidates were co-evaporated with CsI and CeI_3 to prepare a series of Cs_3CeI_6@host films using a three-source co-evaporation system [Figure 1A]. During this screening process, a high-throughput co-evaporation strategy was adopted to rapidly optimize the host-to-inorganic composition for each candidate. The deposition rates were controlled at 0.04 ± 0.002 Å/s for CsI, 0.02 ± 0.002 Å/s for CeI_3, and 1.00 ± 0.200 Å/s for the organic host during the initial comparison. Under 350 nm excitation, films containing carbazole-based hosts showed substantially stronger emission than the other systems [Supplementary Figure 1], indicating that carbazole derivatives are more favorable for constructing efficient emissive films in this material platform.

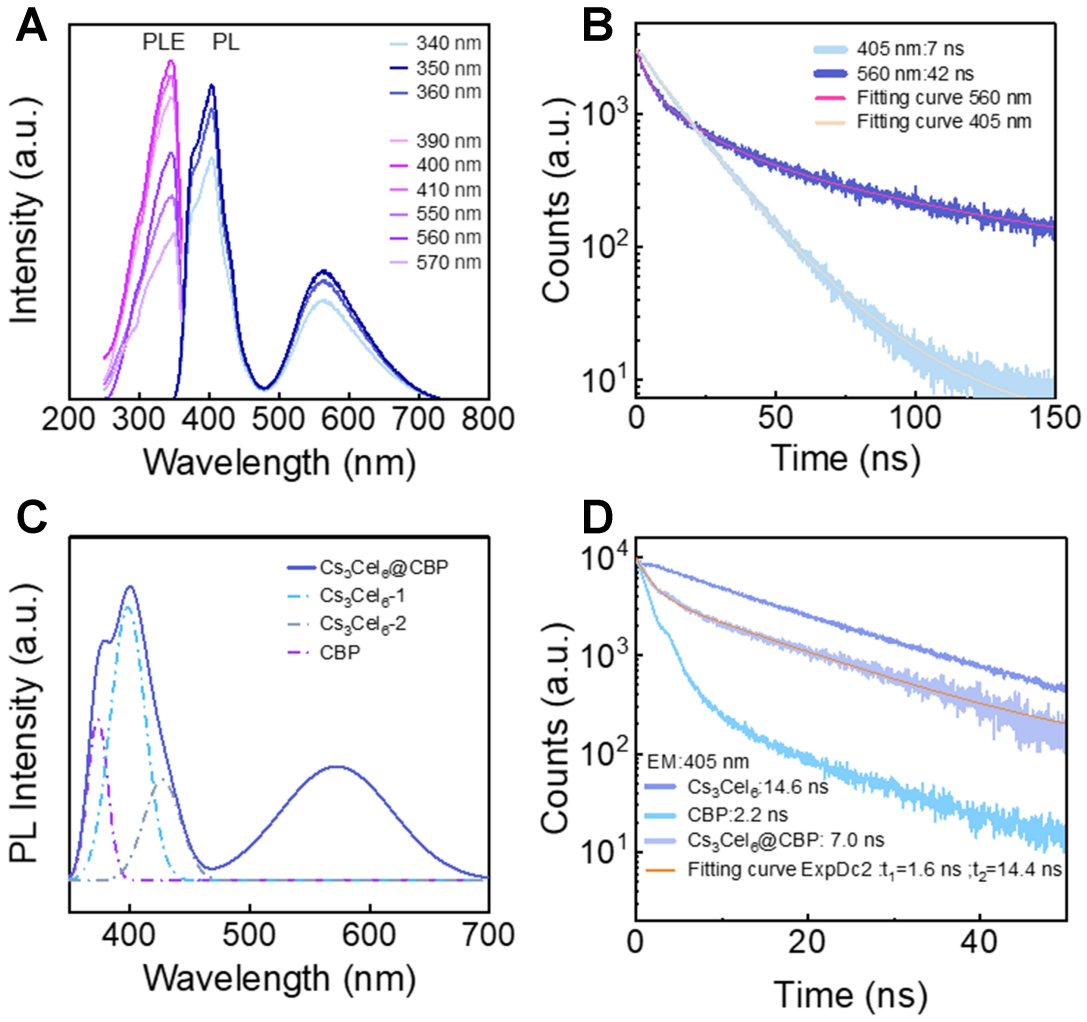

Figure 2. (A) PL spectra excited at different wavelengths and PLE spectra monitored at different emission wavelengths for the Cs_3CeI_6@CBP films; (B) TRPL decay curves of the blue and yellow emission bands in the Cs_3CeI_6@CBP films under 350 nm excitation; (C) Deconvoluted PL spectrum of Cs_3CeI_6@CBP, showing the contributions from Cs_3CeI_6 and CBP in the blue-emission region; Cs_3CeI_6-1 and Cs_3CeI_6-2 represent the characteristic peaks of Cs_3CeI_6 at 400 and 430 nm, respectively; (D) PL decay curves of Cs_3CeI_6, CBP, and Cs_3CeI_6@CBP films under 350 nm excitation. PL: Photoluminescence; PLE: photoluminescence excitation; CBP: 4,4′-Bis(N-carbazolyl)-1,1′-biphenyl; TRPL: time-resolved photoluminescence; EM: emission.

Among the carbazole derivatives, CBP, mCBP, and TCTA were selected for further comparison. Their molecular structures are shown in Supplementary Figure 1. As presented in Figure 1B, the corresponding Cs_3CeI_6@CBP, Cs_3CeI_6@mCBP, and Cs_3CeI_6@TCTA films all exhibit broad visible emission with two distinct peaks, consistent with white-light emission. Among them, the Cs_3CeI_6@CBP film shows the shortest PL lifetimes at both 405 and 560 nm under 350 nm excitation [Figure 1C and D]. This behavior indicates faster excited-state decay dynamics in the CBP-based film. The higher PLQY of Cs_3CeI_6@CBP further supports this conclusion [Supplementary Figure 2 and Supplementary Table 1]. Considering its favorable spectral profile, higher PL efficiency, and suitable electronic properties, CBP was selected as the optimal host for subsequent investigation. We therefore focused on the Cs_3CeI_6@CBP film to examine its emission behavior in detail.

We then investigated the optical properties of the Cs_3CeI_6@CBP film in detail. As shown in Figure 2A, the film exhibits two emission bands centered at 405 and 560 nm. The overall PL profile remains nearly unchanged under different excitation wavelengths, indicating that the two bands are generated within the same emissive system. Consistently, the photoluminescence excitation (PLE) spectra monitored at 390, 400, and 410 nm, as well as at 550, 560, and 570 nm, show very similar shapes, suggesting that the blue and yellow emissions are associated with closely coupled excitation pathways.

TRPL measurements further reveal distinct decay dynamics for the two bands [Figure 2B]. The blue emission at 405 nm exhibits a short lifetime of 7 ns, whereas the yellow emission at 560 nm shows a longer lifetime of 42 ns. This clear difference indicates that the two bands originate from different radiative processes. In addition, both lifetimes are much shorter than those reported for some other single-component white-emissive systems, such as $Cs_2Na_{0.4}Ag_{0.6}InCl_6$ with microsecond-scale decay[9], which indicates faster excited-state decay dynamics.

To clarify the origin of the dual-band emission, we measured the PL spectra of individually evaporated CBP and Cs_3CeI_6 films [Supplementary Figure 3] and performed peak-deconvolution analysis on the Cs_3CeI_6@CBP PL spectrum. The fitted peak positions are consistent with those experimentally observed [Figure 2C], revealing that both Cs_3CeI_6 and CBP contribute to the blue emission, and that the 405 nm peak arises from the superposition of these contributions. Biexponential fitting of the Cs_3CeI_6@CBP blue-band decay yields two lifetimes, τ_1 = 1.6 ns and τ_2 = 14.4 ns, which agree well with the lifetimes of pure CBP (2.2 ns) and pure Cs_3CeI_6 (14.6 ns), respectively [Figure 2D]. The shortened CBP lifetime in the hybrid film confirms the presence of resonant energy transfer from CBP to Cs_3CeI_6, with a calculated energy-transfer efficiency of 27.2%. according to

$$\eta_{ET} = 1 - \tau_{DA}/\tau_D$$

where τ_D and τ_{DA} represent the lifetimes of pristine CBP and the CBP component in the composite film, respectively.

To gain further insight into the emissive film, we next examined its structural and chemical characteristics. TEM shows that Cs_3CeI_6 is formed within the co-evaporated film, with an average size of about 15 nm and uniform distributions of Cs, Ce, and I [Supplementary Figure 4]. High-resolution TEM indicates a preferred orientation along the (2, -1, 2) plane. This result is consistent with the XRD pattern of the film, which agrees well with the simulated pattern derived from Cs_3CeI_6 CIF data [Figure 3A], confirming the formation of crystalline Cs_3CeI_6 nanodomains in the deposited film.

XPS was further employed to probe the chemical environment of Ce^{3+} in pristine Cs_3CeI_6 and Cs_3CeI_6@CBP films. The appearance of an N 1s signal in the survey spectrum of Cs_3CeI_6@CBP confirms successful incorporation of CBP [Figure 3B]. For the pristine Cs_3CeI_6 film, characteristic Ce $3d_{5/2}$ and $3d_{3/2}$ peaks are observed at 886.4 and 904.7 eV, respectively. In contrast, the Cs_3CeI_6@CBP film exhibits additional Ce $3d_{5/2}$ and $3d_{3/2}$ components at 882.4 and 901.2 eV [Figure 3C], suggesting the formation of a modified Ce chemical environment associated with interfacial interaction with CBP. Simultaneously, the I $3d_{5/2}$ peak shifts from 619.1 to 619.7 eV after CBP incorporation [Figure 3D], indicating that the local iodide environment is also affected by CBP incorporation. Together, these results support the presence of interfacial interaction between the inorganic Cs_3CeI_6 component and the organic CBP host.

We next evaluated the influence of CBP concentration on the emissive properties by varying the CBP deposition rate from 1 to 4 Å/s while keeping the CsI and CeI_3 rates fixed at 0.04 and 0.02 Å/s, respectively. As shown in Supplementary Figure 5, increasing the CBP deposition rate leads to a gradual decrease in the blue-emission intensity and a simultaneous increase in the yellow-emission contribution. When the CBP content is too high, intrinsic CBP fluorescence becomes more evident and exciton transfer becomes less complete. When the CBP content is too low, the relative fraction of Cs_3CeI_6 increases, which is unfavorable because it can aggravate concentration quenching. Based on these trends, the deposition rates of 0.04 Å/s for CsI, 0.02 Å/s for CeI_3, and 2 Å/s for CBP were identified as the optimal condition for achieving balanced dual-band emission.

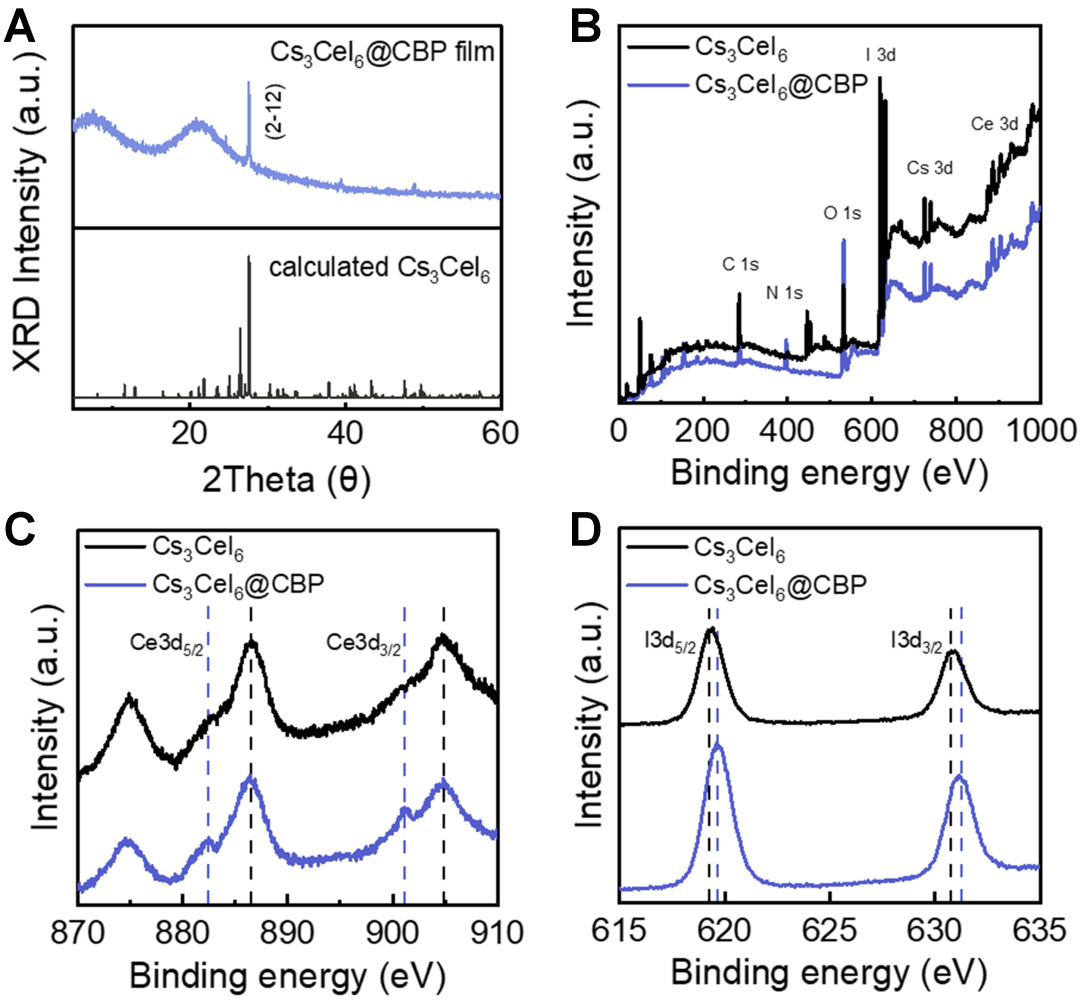

Figure 3. (A) XRD patterns of Cs_3CeI_6@CBP films compared with simulated Cs_3CeI_6; (B) XPS full spectrum of Cs_3CeI_6 and Cs_3CeI_6@CBP films; (C) Ce 3d XPS spectra of Cs_3CeI_6 and Cs_3CeI_6@CBP films; (D) I 3d XPS spectra of Cs_3CeI_6 and Cs_3CeI_6@CBP films. XRD: X-ray diffraction; CBP: 4,4′-Bis(N-carbazolyl)-1,1′-biphenyl; XPS: X-ray photoelectron spectroscopy.

Based on the favorable warm-white emission of the Cs_3CeI_6@CBP film, we fabricated electroluminescent devices using this film as the emissive layer. The device architecture is illustrated in Figure 4A, where TAPC serves as the hole-transport layer, CBP acts as an interfacial layer, and TPBi functions as the electron-transport layer. The initial device, D1, with the structure ITO/HAT-CN (3 nm)/TAPC (40 nm)/Cs_3CeI_6@CBP (30 nm)/TPBi (25 nm)/LiF (2 nm)/Al (100 nm), shows a relatively high turn-on voltage of 7 V [Figure 4B]. To improve charge injection and overall device performance, we further optimized both the transport structure and the emissive-layer composition.

By introducing MoO_3-doped TAPC and inserting a thin CBP transition layer, we obtained the optimized device D2 with the structure ITO/HAT-CN (3 nm)/TAPC:15% MoO_3 (40 nm)/CBP (5 nm)/Cs_3CeI_6@CBP (30 nm)/TPBi (25 nm)/LiF (2 nm)/Al (100 nm). This optimized device exhibits a reduced turn-on voltage of 4 V, a maximum luminance of 2,678 cd/m², and a peak EQE of 2.1% [Figure 4C]. The electroluminescence spectra remain nearly unchanged over the voltage range of 5 to 9 V and closely match the PL spectrum of the film [Figure 4D], indicating stable warm-white emission. The device shows warm-white emission with Commission internationale de l'éclairage (CIE) coordinates of (0.38, 0.39), corresponding to a correlated color temperature of approximately 4,062 K [Figure 4E]. Under constant-current operation at an initial

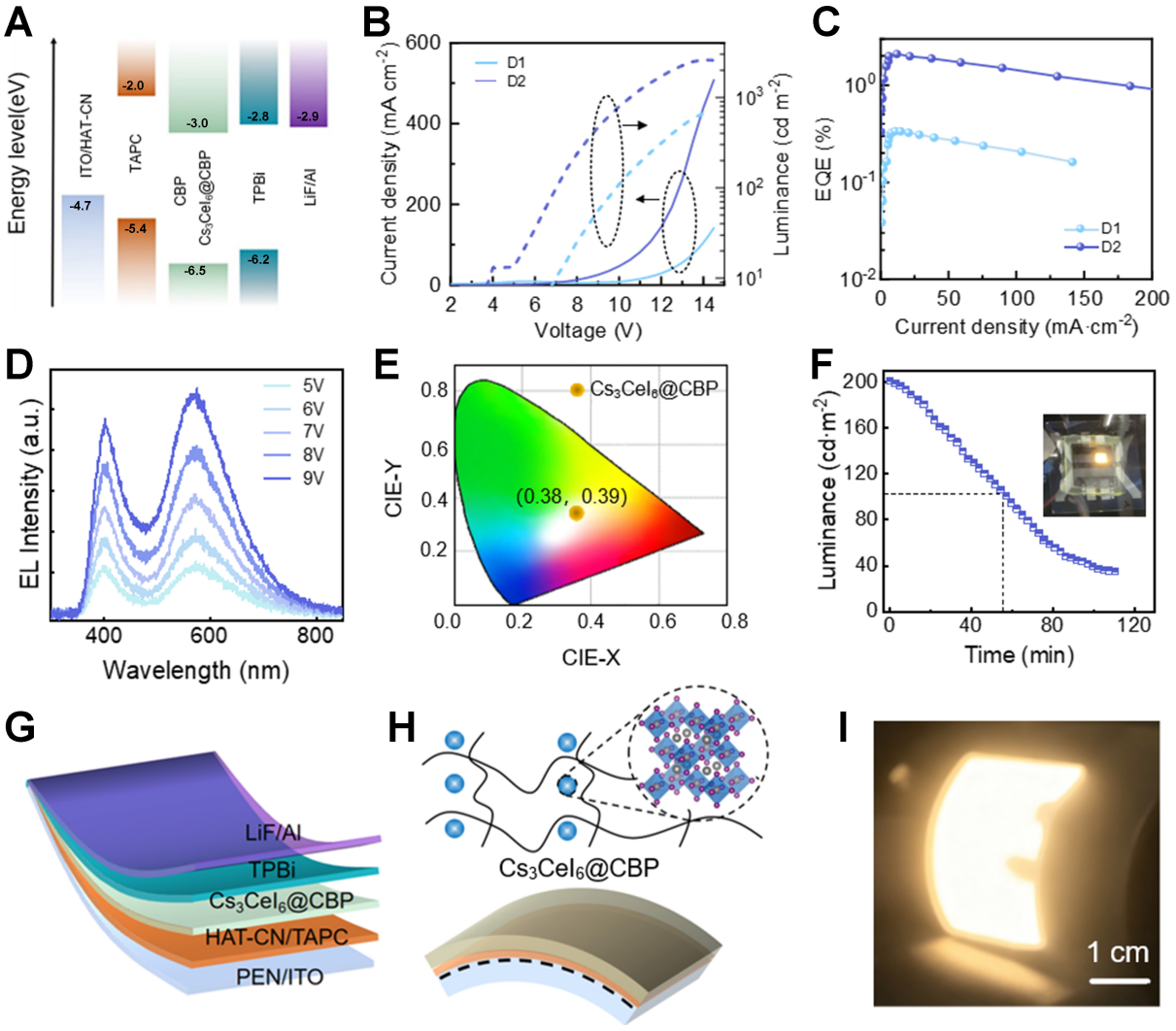

Figure 4. (A) Energy-level diagram and device architecture of the Cs_3CeI_6@CBP electroluminescent device; (B and C) Current density–voltage, luminance–voltage, and EQE–current-density characteristics of Cs_3CeI_6@CBP-based LEDs before (D1) and after (D2) optimization; (D) EL spectra of the optimized device measured at different driving voltages. The ellipses with arrows in (B) indicate the ordinate axes corresponding to the two curves; (E) CIE coordinates of the Cs_3CeI_6@CBP warm-WLEDs; (F) Operational stability of Cs_3CeI_6@CBP warm-WLEDs at an initial luminance of 200 cd/m^2; the inset shows a photograph of the working device; (G) Schematic illustration of the flexible device architecture; (H) Conceptual illustration of the Cs_3CeI_6@CBP emissive layer integrated on a PEN flexible substrate; (I) Photograph of the flexible device under bending condition with bright warm-white electroluminescence. The photographs shown in (F) and (I) were taken by the authors. CBP: 4,4′-Bis(N-carbazolyl)-1,1′-biphenyl; EQE: external quantum efficiency; LEDs: light-emitting diodes; EL: electroluminescence; CIE: Commission internationale de l'éclairage; WLEDs: white light-emitting diodes; PEN: polyethylene naphthalate; ITO: indium tin oxide; HAT-CN: 2,3,6,7,10,11-Hexacyano-1,4,5,8,9,12-hexaazatriphenylene; TAPC: 1-Bis[4-[N,N-di(4-tolyl)amino]phenyl]-cyclohexane; TPBi: 1,3,5-Tris(1-phenyl-1H-benzimidazol-2-yl)benzene; LiF: lithium fluoride.

luminance of 200 cd/m^2, the device shows a T_{50} lifetime of 59.7 min [Figure 4F]. Devices with different emissive-layer ratios also exhibit differences in performance [Supplementary Table 2]. A comparison of device performance with previously reported WLEDs is summarized in Supplementary Table 3. The EQE and operational lifetime remain limited compared with practical requirements. These limitations are likely associated with the intrinsic difficulty of electrically exciting Ce^{3+} centers, since the localized 4f orbitals are shielded by outer 5s/5p orbitals, which can limit direct carrier injection and energy utilization. In addition, incomplete energy transfer from CBP to Cs_3CeI_6, nonradiative losses, and unbalanced electron–hole injection and transport arising from the present device architecture collectively degrade the overall device performance. To further illustrate the applicability of this material system in flexible optoelectronics, we

constructed a flexible device concept on a polyethylene naphthalate (PEN) substrate based on the same functional layer configuration and Cs_3CeI_6@CBP emissive film [Figure 4G and H]. The corresponding flexible device exhibits bright warm-white electroluminescence under bending conditions [Figure 4I], serving as an initial proof-of-concept demonstration of the compatibility of the co-evaporated emissive layer with flexible substrates. The EL spectrum of the flexible device remains nearly unchanged after bending, suggesting good spectral stability under mechanical deformation [Supplementary Figure 6A]. Quantitative bending tests further show that the device retains over 94% of its initial luminance after 100 bending cycles at a bending radius of 6 mm, and still maintains approximately 85% after 200 cycles [Supplementary Figure 6B], with L_0 set to approximately 100 cd/m^2. These results, together with the solvent-free and thickness-controllable nature of vapor deposition, highlight the potential of these cerium-based halide-organic composites for future flexible light-emitting applications. By tuning the deposition-rate ratio of CsI, CeI_3, and CBP, the electroluminescence spectra and CIE coordinates can also be modulated, enabling color-adjustable devices [Supplementary Figures 7 and 8].

CONCLUSION

In summary, we have demonstrated vapor-deposited Cs_3CeI_6@CBP nanocrystal films for warm-white electroluminescence. The co-evaporated films exhibit dual-band visible emission, with a blue band centered at 405 nm and a yellow band centered at 560 nm. Spectroscopic analysis suggests that the blue emission arises from the combined contributions of the Cs_3CeI_6 component and CBP fluorescence, while the yellow emission is associated with Ce^{3+}-centered 5d–4f emission under a modified local environment induced by interfacial interaction with CBP. Based on these films, warm-WLEDs were realized with Commission Internationale de l'Eclairage coordinates of (0.38, 0.39), a peak external quantum efficiency of 2.1%, a maximum luminance of 2,678 cd/m^2, and stable electroluminescence over a broad operating-voltage range. The relatively modest EQE is mainly attributed to incomplete energy transfer from CBP to Cs_3CeI_6, charge imbalance, and non-radiative recombination within the hybrid emissive layer. In addition, the flexible electroluminescent device demonstration further reveals the applicability of these nanocrystal films in flexible light-emitting devices. This work provides an effective vapor-deposition route for cerium-based halide-organic composites and offers useful guidance for the development of flexible warm-WLEDs.

DECLARATIONS

Acknowledgment

The authors from HUST acknowledge the support from the Center for Nanoscale Characterization and Devices, the Analytical and Testing Center of HUST, and the Instruments Sharing Platform at the School of Optical and Electronic Information of HUST.

Authors' contributions

Supervised the whole project: Tang, J.; Luo, J.; Du, J.
Designed and performed most of the experiments, characterizations and analysis: Wu, X.; Li, J.
Involved in the EL device fabrication and optimization: Li, Z.
Provided the optical characterizations: Luo, Y.; Yang, L.
Organized the outline of this manuscript: Luo, J.
Wrote the paper: Luo, J.; Wu, X.; Li, J.; Du, J.; Tang, J.
All authors discussed the results and commented on the manuscript.

Availability of data and materials

The data supporting the findings of this study are presented in this manuscript and Supplementary Materials.

AI and AI-assisted tools statement

During the preparation of this manuscript, ChatGPT (OpenAI, GPT-5.5,2026-04-23) was used only for language polishing; Gemini (Gemini 3.6 Flash,2026-07-21) was used to generate the conceptual illustration of the white-light flexible display for the graphical abstract. The tool did not influence the study design, data

collection, analysis, interpretation, or the scientific content of the work. All authors take full responsibility for the accuracy, integrity, and final content of the manuscript.

Financial support and sponsorship

This work was supported by the National Key R&D Program of China (2023YFB3608900, 2024YFA1209503) and the National Natural Science Foundation of China (62322505, 62374069 62304086), the key R&D program from Hubei Province (2024BAA004, 2023BAB102), and the Interdisciplinary program of Wuhan National High Magnetic Field Center (WHMFC2025018) of Huazhong University of Science and Technology.

Conflicts of interest

All authors declared that there are no conflicts of interest.

Ethical approval and consent to participate

Not applicable.

Consent for publication

Not applicable.

Supplementary Materials

Supplementary Materials

REFERENCES

1. Cho, J.; Park, J. H.; Kim, J. K.; Schubert, E. F. White light-emitting diodes: history, progress, and future. *Laser. Photonics. Rev.* **2017**, *11*, 1600147. DOI
2. Shirasaki, Y.; Supran, G. J.; Bawendi, M. G.; Bulović, V. Emergence of colloidal quantum-dot light-emitting technologies. *Nat. Photon.* **2013**, *7*, 13–23. DOI
3. Pimputkar, S.; Speck, J. S.; DenBaars. S. P.; Nkamura, S. Prospects for LED lighting. *Nat. Photon.* **2009**, *3*, 180-2. DOI
4. Tsao, J. Y.; Crawford, M. H.; Coltrin, M. E.; et al. Toward smart and ultra-efficient solid-state lighting. *Adv. Opt. Mater.* **2014**, *2*, 809-36. DOI
5. Teng, Q.; Tan, Q.; Hou, M.; Zhang, J.; Yuan, F. Bright and stable zero-dimensional hexagonal organic–inorganic tin iodide perovskites for high color rendering index white light-emitting diodes. *ACS Energy Lett.* **2025**, *10*, 3691–9. DOI
6. Kido, J.; Kimura, M.; Nagai, K. Multilayer white light-emitting organic electroluminescent device. *Science* **1995**, *267*, 1332-4. DOI PubMed
7. Coe, S.; Woo, W. K.; Bawendi, M.; Bulović, V. Electroluminescence from single monolayers of nanocrystals in molecular organic devices. *Nature* 2002;420:800-3. DOI
8. Zhang, M.; Zheng, C. J.; Wang, K.; et al. Efficient and stable single-emitting-layer white organic light-emitting diodes by employing all thermally activated delayed fluorescence emitters. *Org. Electron.* **2022**, *101*, 106415. DOI
9. Luo, J.; Wang, X.; Li, S.; et al. Efficient and stable emission of warm-white light from lead-free halide double perovskites. *Nature* **2018**, *563*, 541-5. DOI
10. Sun, R.; Lu, P.; Zhou, D.; et al. Samarium-doped metal halide perovskite nanocrystals for single-component electroluminescent white light-emitting diodes. *ACS. Energy. Lett.* **2020**, *5*, 2131-9. DOI
11. Li, X.; Cui, J.; Ba, Q.; et al. Multiphotoluminescence from a triphenylamine derivative and its application in white organic light-emitting diodes based on a single emissive layer. *Adv. Mater.* **2019**, *31*, 1900613. DOI
12. Ma, Z.; Shi, Z.; Qin, C.; et al. Stable yellow light-emitting devices based on ternary copper halides with broadband emissive self-trapped excitons. *ACS. Nano.* **2020**, *14*, 4475-86. DOI
13. Ilmi, R.; Khan, M. S.; Sun, W.; Zhou, L.; Wong, W. Y.; Raithby, P. R. A single component white electroluminescent device fabricated from a metallo-organic terbium complex. *J. Mater. Chem. C* **2019**, *7*, 13966-75. DOI
14. Jo, D. Y.; Kim, H. M.; Park, G. M.; et al. Unity quantum yield of InP/ZnSe/ZnS quantum dots enabled by Zn halide-derived hybrid shelling approach. *Soft. Sci.* **2024**, *4*, 27. DOI

15. Wu, T. L.; Huang, M. J.; Lin, C. C.; et al. Diboron compound-based organic light-emitting diodes with high efficiency and reduced efficiency roll-off. *Nat. Photon.* **2018**, *12*, 235-40. DOI
16. Yang, L.; Du, H.; Li, J.; et al. Efficient deep-blue electroluminescence from Ce-based metal halide. *Nat. Commun.* **2024**, *15*, 6240. DOI PubMed PMC
17. Li, J.; Wang, L.; Zhao, Z.; et al. Highly efficient and air-stable Eu(II)-containing azacryptates ready for organic light-emitting diodes. *Nat. Commun.* **2020**, *11*, 5218. DOI
18. Zhou, J.; Zheng, G.; Liu, X.; Dong, G.; Qiu, J. Defect engineering in lanthanide doped luminescent materials. *Coord. Chem. Rev.* **2021**, *448*, 214178. DOI
19. Bünzli, J. C. G. On the design of highly luminescent lanthanide complexes. *Coord. Chem. Rev.* **2015**, *293–4*, 19–47. DOI
20. Tiedje, T.; Colbow, K. M.; Gao, Y.; Dahn, J. R.; Reimers, J. N.; Houghton, D. C. Role of Coulomb repulsion in 4*f* orbitals in electrical excitation of rare-earth impurities in semiconductors. *Appl. Phys. Lett.* **1992**, *61*, 1296-7. DOI
21. Seol, M. J.; Jeong, J.; Kim, S. Y. Efficiency enhancement of thermal-evaporated perovskite light-emitting diodes through process optimization and additive engineering. *Energy. Mater.* **2026**, *6*, 600018. DOI
22. Sun, H.; Yang, X.; Li, P.; et al. Solution synthesis and light-emitting applications of one-dimensional lead-free cerium(III) metal halides. *Nano. Lett.* **2024**, *24*, 10355-61. DOI
23. Lindahl, J.; Zimmermann, U.; Szaniawski, P.; et al. Inline Cu(In,Ga)Se_2 co-evaporation for high-efficiency solar cells and modules. *IEEE J. Photovolt.* **2013**, *3*, 1100–5. https://ieeexplore.ieee.org/stamp/stamp.jsp?arnumber=6504703. (accessed 2026-09-04).
24. Chen, H.; Zhu, L.; Xue, C.; et al. Efficient and bright warm-white electroluminescence from lead-free metal halides. *Nat. Commun.* **2021**, *12*, 1421. DOI PubMed PMC
25. Yao, E. P.; Yang, Z.; Meng, L.; et al. High-brightness blue and white LEDs based on inorganic perovskite nanocrystals. *Adv. Mater.* **2017**, *29*, 1606859. DOI PubMed
26. Noto, M.; Gotou, Y.; Era, M. Red electroluminescence from divalent europium iodide nano-particle doped in organic-semiconductor. *Thin Solid Films* **2003**, *438–9*, 153–6. DOI
27. Era, M.; Noto, M.; Goto, Y. Electroluminescence from organic–inorganic hybrid structures. *J. Lumin.* **2013**, *141*, 6-8. DOI
28. Keum, K.; Yang, S.; Kim, K. S.; Park, S. K.; Kim, Y. H. Recent progress of stretchable displays: a comprehensive review of materials, device architectures, and applications. *Soft. Sci.* **2024**, *4*, 34. DOI